Radiometric dating of recent sediments: beyond the boundary conditions

José-María Abril, Foued Gharbi

Abstract Most mathematical models for radiometric dating of recent sediments are particular solutions of a unique physical problem: the advective–diffusive transport of a particle-bound radiotracer within a sediment profile that undergoes accretion. Regardless of the particular assumptions about fluxes, sedimentation rates and the diffusion term, all models assume ideal deposition as a boundary condition at the sediment water interface, i.e. new radioactive input will be deposited above the previously existing material. In sediments with very high porosities, this assumption may be unrealistic, because a fraction of the incoming flux may penetrate rapidly through the connected pore spaces. This process will be referred to as non-ideal deposition. This paper reviews evidence from literature data, discusses the basic processes involved, and establishes the mathematical basis to incorporate non-ideal deposition into one-phase radiometric dating models, as depth-distributed local sources. Through analytical and numerical solutions, this work demonstrates that such penetration patterns can explain excess ^{210}Pb subsurface maxima, often observed in sediment cores, as well as penetration of ^{137}Cs to depths greater than expected from sedimentation rates and diffusion. These ideas are illustrated using examples from the literature in which sediment porosities were >90 %. Implications for radiometric dating include: (1) spurious accelerations in sedimentation rate inferred when applying the constant rate of supply model, and (2) erroneous chronologies, developed when using the maximum depth at which ^{137}Cs can be measured as a chronostratigraphic marker.

Keywords Radiometric dating · Boundary conditions · Non-ideal deposition · ^{210}Pb subsurface maxima · Non-diffusive depth penetration

J.-M. Abril (✉)
Dpto. Física Aplicada I, Universidad de Sevilla, ETSIA, Ctra Utrera Km 1 m, 41013 Seville, Spain
e-mail: jmabril@us.es

F. Gharbi
National Center of Nuclear Sciences and Technology, Sidi Thabet, P.C., 2020 Tunis, Tunisia

Introduction

Radiometric dating of recent lake deposits can provide sedimentation rates and dates, which are key to understanding the chronology of historical environmental events preserved in the sediments. Koide et al. (1972) and later Koide et al. (1973) demonstrated the use of excess ^{210}Pb (^{210}Pb$_{exc}$) activities for establishing radiogeochronology in marine sediments. Since then, ^{210}Pb$_{exc}$, along with bomb-fallout radionuclides, has been widely used for dating both marine and freshwater deposits, fostered by the development of different radiometric dating models (Appleby and Oldfield 1978; Robbins 1978; Christensen 1982; Abril et al. 1992; Fukumori et al. 1992; Abril 2004; Meysman et al. 2005; Laissaoui et al. 2008).

Radiometric dating models have a set of assumptions about the expected functioning of the sedimentary system, e.g. inputs of $^{210}Pb_{exc}$ and/or sedimentation rates are constant or vary, and diffusion occurs or does not occur. These assumptions allow us to find particular solutions from the general and unique physical problem of mass conservation for solids and for the particle-associated tracers, in sediments that undergo accretion and compaction. In terms of the mass depth variable, m [g dry matter cm^{-2} lying above any given sediment horizon at depth z, measured below the sediment water interface (SWI)], and for steady-state bulk density profiles, this equation can be written as (Abril 2003a):

$$\frac{\partial A}{\partial t} = -\lambda A - w\frac{\partial A}{\partial m} + \frac{\partial}{\partial m}\left(k_m\frac{\partial A}{\partial m}\right), \tag{1}$$

in which A is the specific activity of the studied radionuclide, λ its radioactive decay constant, w the mass sedimentation rate as defined by Abril (2003a), and k_m is an effective diffusion coefficient. Steady state bulk density profiles can exist under variable sedimentation rates when the conductivity of solids co-varies with the rates (Abril 2011). Under unsteady compaction, Eq. 1 has to be rewritten and coupled with the equation for mass conservation of solids given by the theory of early compaction (Abril 2003a, 2011).

Equation 1 assumes that radionuclides are particle-bound, that the sediment can be modeled as a continuous medium, and the time scale of interest is typically several decades. The diffusion term accounts for random motions of individual particles, with a null net mass flow. When required, we can improve our mathematical description by using a two-phase model (solids and pore-water) assuming local equilibrium for the solid-to-liquid partitioning of the tracer (Robbins and Jasinski 1995).

To properly define the mathematical problem, Eq. 1 requires initial and boundary conditions. In most cases, $A(m, t) = 0$ can be selected for both man-made radionuclides and $^{210}Pb_{exc}$. In this latter case, equations have to be solved for time scales large enough to allow steady-state solutions. The boundary condition on the continuity of flux at the SWI is imposed by the equation:

$$\phi(t) = -k_m\frac{\partial A}{\partial m}\bigg|_{m=0} + wA(0,t), \tag{2}$$

in which $\phi(t)$ is the flux of the studied radionuclide (Bq per unit area per unit time) entering the sediment at the

SWI, which can be different from the local atmospheric deposition rate if processes in the catchment and/or water column are relevant. For great depths, the following boundary condition applies:

$$\lim_{m\to\infty} A(m,t) = 0 \tag{3}$$

If there is no diffusion ($k_m = 0$), Eq. 2 leads to $A(0, t) = \phi/w$, which contains the particular case of the boundary conditions used in the constant flux-constant sedimentation rate (CF-CSR) model.

Equation 1 can be integrated by mass depth (from the SWI to $m \to \infty$) to yield inventories. The constant rate of supply (CRS) model arises then as a particular solution under conditions of non-diffusion and constant flux. Note that Eq. 2 then implies steady-state inventories:

$$\sum_m = \sum_0 e^{-\lambda T(m)}, \tag{4}$$

in which $\sum_0$ and $\sum_m$ are the inventories below the SWI and the horizon at mass depth m, respectively, and $T(m)$ is the age of the sediment horizon now at mass depth m. The CRS model can also be expressed using the depth variable, z.

The assumption of ideal deposition, i.e. that any new radioactive input must necessarily be deposited above previously existing material, is implicitly incorporated in the boundary conditions (Eq. 2), and its effects are clearly observed in the fundamental equation of the CRS model (Eq. 4). In terms of mass balance for a differential sediment layer of mass thickness dm, placed at the SWI, it receives a flux $\phi(t)$, whereas its lower boundary, at $m = dm$, is crossed by an advective–diffusive flux, the net balance being the rate of change of the activity. The penetration of radioactive fluxes with depth depends, consequently, on advective and diffusive transport, the latter forced by spatial gradients of concentration.

The assumption of ideal deposition of settling particulate matter and the activity fluxes seems quite obvious, but may not always be correct, particularly in sediments with very high porosities (>90 %), like the cores studied in this work. A field-tracer experiment was initiated unintentionally, in April 1986, with the Chernobyl accident. A review of important studies carried out at that time (Holby and Evans 1996; Petersen et al. 1990; Kramer et al. 1991) provides insight into how fluxes were deposited onto (and into) the surface sediments. In most cases rapid depth

distributions were quite noticeable. Robbins and Jasinski ([1995](#)) found that within 4 months of the fallout from Chernobyl, [134]Cs had penetrated down to about 10 cm in one sediment core from Lake Sniardwy (Poland) and, in cores collected from three sites a year later, had penetrated to between 14 and 24 cm. Large depths of Cs isotope penetration were also observed in sediments from the Baltic Sea and could not be explained by bioturbation or by diffusion (Holby and Evans [1996](#)). In some cases, diffusion models provided a generally satisfactory description of the data, but they failed to explain the small tails of radiocesium that penetrated to greater depths (Robbins and Jasinski [1995](#)). Furthermore, when applying these diffusion models to a sequence of cores taken on different dates, it was necessary to use mixing coefficient values that decreased with time. These findings suggest that initial diffusion coefficients were overestimated in an attempt to account for other processes that contributed to the rapid distribution of radionuclides to greater depth.

Rapid distribution to depth of a fraction of incoming flux cannot be reproduced under the assumptions and simplifications involved in one-phase and two-phase equilibrium models. We refer to this effect as "non-ideal deposition." This paper presents evidence from the literature that non-ideal deposition occurs, and provides a critical review of the basic processes involved.

First, it will be helpful to explain the mathematical basis for incorporating non-ideal deposition into one-phase radiometric dating models. This will allow us to explain the often-observed "penetrating tails" in ^{137}Cs profiles and the subsurface maxima in [210]Pb$_{exc}$ profiles (Sugai et al. [1994](#); Baskaran and Naidu [1995](#); Fuller et al. [1999](#); Belluci et al. [2007](#)). Although the main purpose of this paper is not development of a new dating model, the subject has implications for radiometric dating of recent sediments. This is discussed using examples from literature data.

Materials and methods

Non-ideal deposition in one-phase radiometric dating models

It is assumed that a fraction, g, of the incoming activity flux will be distributed within a certain mass depth in the sediment, while the remaining fraction $(1 - g)$ will be deposited at the SWI. Possible physical and chemical processes accounting for such fast redistribution in depth will be discussed further, but do not necessarily violate the steady state for bulk density profiles, nor the formation of varves. The process of flux distribution with depth is assumed to be fast in relation to the time scales involved in the radiogeochronology. It can be modelled as a local (depth-distributed) source term, $s(m)$ in Eq. [1](#), maintaining the assumption of a continuous medium:

$$\frac{\partial A}{\partial t} = -\lambda A - w\frac{\partial A}{\partial m} + \frac{\partial}{\partial m}\left(k_m\frac{\partial A}{\partial m}\right) + s(m) \qquad (5)$$

The boundary condition is then rewritten as follows:

$$(1 - g)\phi(t) = -k_m\frac{\partial A}{\partial m}\bigg|_{m=0} + wA(0, t) \qquad (6)$$

in which the local source term must satisfy the following condition:

$$\int_0^\infty s(m)dm = g\phi(t) \qquad (7)$$

Different depth-distribution functions can be established, but the simplest one that will allow us to pursue analytical solutions is exponential penetration with a scaling factor α:

$$s(m) = s_0 e^{-\alpha m} \qquad (8)$$

The closure condition of Eq. [7](#) provides $s_0 = \alpha g\phi(t)$. For the simplest case of constant fluxes (often assumed for [210]Pb$_{exc}$) and constant sedimentation rates, without diffusion, the steady-state solution $\left(\frac{\partial A}{\partial t} = 0\right)$ of Eq. [5](#) is

$$A(m) = C_1 e^{-\lambda\frac{m}{w}} + C_2 e^{-\alpha m} \qquad (9a)$$

$$C_2 = \frac{-\alpha g\phi}{\alpha w - \lambda}; \quad C_1 = \frac{(1 - g)\phi}{w} - C_2 \qquad (9b)$$

We note that for $g = 0$, $C_2 = 0$, leading to the known solution for the CF-CSR model. On the other hand, at the SWI the activity concentration is $(1 - g)$ times the one expected from the CF-CSR model. Consequently, the parameter g can be deduced from the observed drop in activity concentration with respect to the expected value at the SWI from the CF-CSR model. Finally, if $\alpha \gg \lambda/w$, the second exponent vanishes faster, and the first term governs

the resulting trend. Thus, the conventional fit to an exponential function, by excluding the uppermost region in the profile, can provide a good estimate of the sedimentation rate, and consequently, of the expected activity at the SWI, using the CF-CSR model. We note that the profile is steady-state. Thus, the constant flux can be found from the total inventory ($\phi = \lambda \Sigma_0$). Equation 9a, 9b can explain the occurrence of subsurface maxima in $^{210}Pb_{exc}$ profiles, which are sometimes pronounced, depending on the values of g and α in Fig. 1. This equation can be used to solve α from the observed position and magnitude of the subsurface peak, but numerical fits are equally applicable.

The effect of non-ideal deposition in ^{210}Pb chronologies can be understood, as a first approach, from Eq. 9a, 9b. Deviations from CF-CSR chronologies are greater for small α values (larger penetration depths), larger g values (i.e. higher fraction of flux being deposited non-ideally) and larger sedimentation rates.

Let us consider a Gaussian pulse of a non-radioactive material that enters at time t_i into sediment under ideal deposition conditions, with a constant sedimentation rate and no diffusion. At any time, $t > t_i$, the mass depth profile for the speci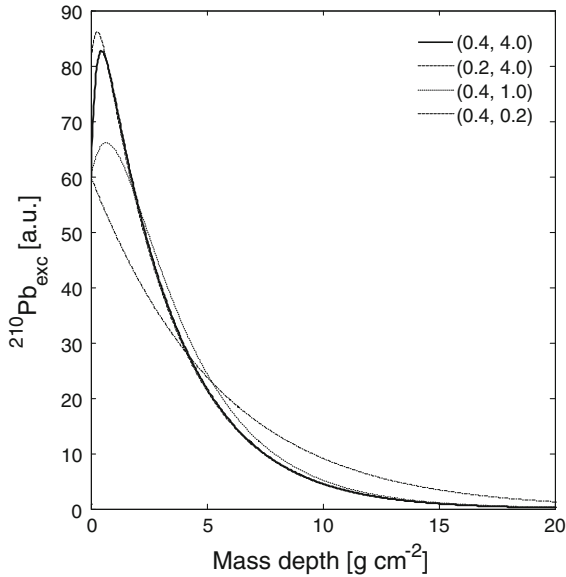fic concentration of this pollutant will be Gaussian-like, with the centroid at mass depth $m = (t - t_i)\,w$ and with sigma $\sigma_m = \sigma_t w$. Figure 2 shows the corresponding numerical and analytical solutions for a particular set of parameters. This serves to demonstrate the use of the monotonic second-order upstream (MSOU) numerical scheme (Periáñez 2005) to deal with numerical dispersion under these particular conditions in which steep gradients in concentration occur. In the same figure, the numerical solutions are plotted for a situation of non-ideal deposition, following Eq. 8, for radioactive and non-radioactive tracers. Non-ideal deposition produces tails that penetrate into the sediment deeper than expected from the sedimentation rates. The non-symmetric pattern also shows that this situation is radically different from one with constant diffusion.

Results

Evidence of non-ideal deposition (Chernobyl fallout radionuclides)

The paper by Robbins and Jasinski (1995) closely corresponds to the ideal situation depicted in Fig. 2.
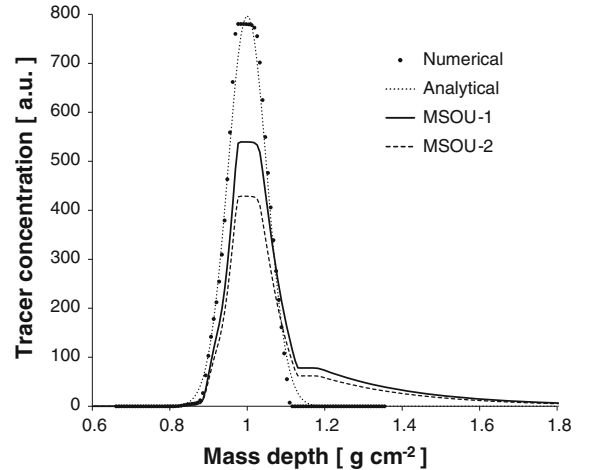

Fig. 1 Analytical solutions given by Eq. 9a, 9b (steady state under constant rate of supply of excess ^{210}Pb, constant sedimentation rate of 0.1 g cm^{-2} year^{-1}, without diffusion). Activity concentrations are expressed in arbitrary units (a.u.). Different curves correspond to the given values of g and α, the latter in units of cm^2 g^{-1}. The last curve is indistinguishable from an ideal exponential decay

Fig. 2 Numerical and analytical solutions (at $t = 12$ year) for a Gaussian pulse ($t_i = 2$ year, $\sigma_t = 0.5$ year) of a non-radioactive pollutant that is incorporated into a sediment (under ideal deposition) that accretes with a constant sedimentation rate $w = 0.1$ g cm^{-2} year^{-1} without diffusion. The figure also shows the numerical solution with the MSOU scheme under non-ideal deposition, with $s(m)$ given by Eq. 8 with $g = 0.4$ and $\alpha = 4.0$ g^{-1} cm^2 (MSOU-1), and when the radioactive decay (the one for ^{137}Cs) is considered (MSOU-2). Activity concentrations are provided in arbitrary units (a.u.)
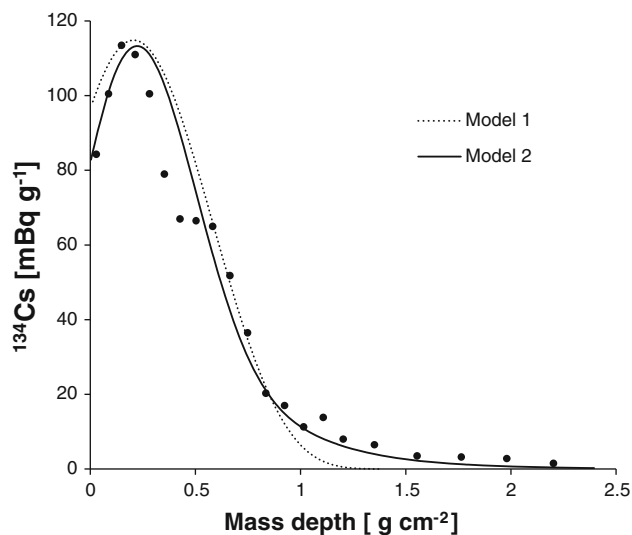
Fig. 3 Distribution of ^{134}Cs in a core from Lake Sniardwy, Poland (data from Robbins and Jasinski 1995, with typical analytical uncertainties <5 %; sampled in summer 1987). Model-1 reproduces the numerical solution provided by these authors (using a two-phase equilibrium model) governed by a depth-dependent coefficient for diffusive mixing of bulk sediment (10 cm^2 year^{-1} for the upper 15 cm, dropping to zero below this depth). Model-2 combines the previous diffusion model with non-ideal deposition given by Eq. 8 ($g = 0.4$, $\alpha = 2.5$ g^{-1} cm^2) and a value for the diffusion coefficient 40 % lower than in Model-1

Figure 3 shows the ^{134}Cs profile they measured in a sediment core from Lake Sniardwy, Poland, sampled in summer 1987 (Site I 8/87). Porosity was >95 % in the top 30 cm, with a value of 97.5 % at the SWI. They applied a two-phase model, assuming local equilibrium with constant k_d, derived from their own sorption experiments. Because of the large value of k_d (4.3×10^3 and 6.3×10^3 ml g^{-1} for contact times of 130 days and 1.12 years, respectively), molecular-scale tracer diffusion had a negligible effect on calculated profiles. The best fit to data, reproduced as Model-1 in Fig. 3, was obtained assuming the profile was governed by a bulk sediment mixing coefficient of 10 cm^2 year^{-1} that affected both solids and pore water and was constant in the top 15 cm, and decreased to zero below. It was justified by the presence of *Oligochaeta* worms. The model provided a generally good description of the data, but failed to explain the penetrating tail of ^{134}Cs.

Model-2 combines the previous diffusion model with non-ideal deposition given by Eq. 8 ($g = 0.4$, $\alpha = 2.5$ g^{-1} cm^2), and a value for the diffusion coefficient that is 40 % lower than in Model-1 (Fig. 3). Overestimated diffusion seems to partly account for the observed profile, except the deeper tail, when only one

date of observation (measurements) is available. Thus, to explain the activity profiles for cores sampled at different times (1986, 1987, 1988) it was necessary to use values of the mixing coefficient that decreased with time (Robbins and Jasinski 1995).

Holby and Evans (1996) studied the depth distributions of radionuclides following the Chernobyl fallout in the bottom sediments of Gälve Bay, southern Bothnian Sea (60°44.15′N, 17°12.10′E, 35 m depth). A sediment core was collected in October 1988 and a second one in June 1991. Water content was 86 % in the 0–2 cm layer. The sediment accumulation rate in this area was about 1 mm year^{-1} ($w \sim 0.015$ g cm^{-2} year^{-1}). The nuclide concentrations were almost constant down to about 8 cm. The authors showed that the calculated diffusivity through the porous sediment was much below those observed. Consequently, diffusion alone could not account for the observed distribution pattern. The authors used a constant-diffusion model, calculated as the analytical solution of an exponential decay function, resulting in a model deviating from the observed pattern. There were few macrobenthic organisms and the bioturbated zone, if it existed, could not have extended deeper than 5 cm. Vertical mixing of pore water could not be explained by bioturbation.

Figure 4 shows the normalized (to their "plateau" value) distributions for ^{137}Cs and ^{134}Cs versus mass depth for the two cores. Depth penetration patterns were essentially equal for both cores and both dates.

The ^{137}Cs inventory, referred to the same date of 1988, in the core sampled in June 1991, was 42 % of the corresponding value for the core sampled in 1988. As the authors pointed out, because of the heterogeneity of the sedimentary environment, it may not be possible to draw general conclusions about net changes in radionuclide contents based on two successive samplings. Nevertheless, Eq. 1, with boundary conditions given in Eqs. 2 and 3, provides suitable solutions using a depth-dependent diffusion coefficient. Thus, the curves in Fig. 4 show the numerical solution obtained by using a Gaussian source, providing the whole inventory in a very short time ($\sigma_t = 0.05$ year was used), $w = 0.015$ g cm^{-2} year^{-1}, and an effective diffusion coefficient (in units of g^2 cm^{-4} year^{-1} from Eq. 5) varying with mass depth as:

$$k_m = \frac{k_0}{1 + e^{\beta(m-m_a)}}, \tag{10}$$

with $k_0 = 0.45$, $m_a = 1.7$ g cm^{-2} and $\beta = 1.2$ g^{-1} cm^2. Diffusion is almost constant over a mass depth m_a
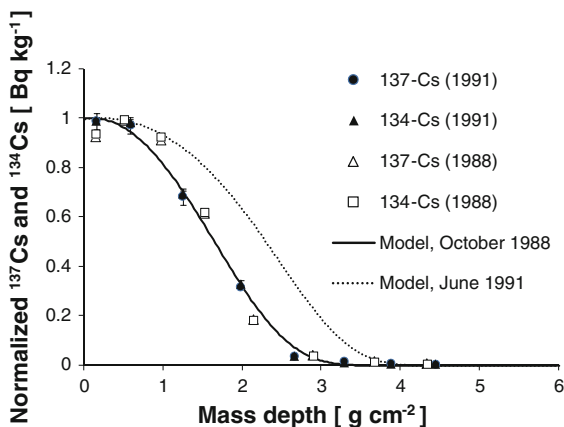

Fig. 4 Normalized to their maximum value, ^{137}Cs and ^{134}Cs distributions in two sediment cores from Gälve Bay, southern Bothnian Sea (60°44.15′N, 17°12.10′E, 35 m depth), sampled in October 1988 and June 1991 (data from Holby and Evans 1996, with 1 σ analytical error bars). The continuous lines correspond to the normalized (to their maximum) numerical solutions of Eqs. 1–3, simulating the Chernobyl input as a Gaussian source providing the total inventory with $\sigma_t = 0.05$ year, $w = 0.015$ g cm^{-2} year^{-1}, and an effective diffusion coefficient given by Eq. 10, with $k_0 = 0.45$ g^2 cm^{-4} year^{-1}, $m_a = 1.7$ g cm^{-2} and $\beta = 1.2$ g^{-1} cm^2, and plotted for the two dates of sampling

and then drops to zero with a scaling factor β. Model-1988 shows the normalized distribution for the first date of sampling, which reasonably follows the observed pattern. Model-1991 corresponds to the normalized solution for the second date of sampling, which clearly fails to explain the observed distribution. In other words, whereas diffusion was high (Eq. 10) for the period 1986–1988, it must have been near zero for the period 1988–1991 to explain the corresponding profiles. Thus, the assumption of ideal deposition of fluxes is inconsistent in this case, because it arbitrarily requires changing diffusion coefficients with depth and time.

Kinetic reactive transport processes

Kinetic reactive transport processes fall beyond the capabilities of one- and two-phase equilibrium models. These processes, among others, could contribute to rapid distribution over depth of a fraction of incoming fluxes.

A radiotracer can attach to different sites within solid particles and/or can form bonds with different strengths that can be identified as different solid phases. According to Evans et al. (1983), ^{137}Cs can attach to: (1) surface and planar sites, from which it is generally exchangeable by all cations, (2) wedge sites, where exchange is limited to cations of similar size and charge, and (3) internal sites, from which it is not readily exchangeable. The kinetics of uptake can then be described by a set of linear transfer equations with constant coefficients (El-Mrabet et al. 2001; Barros et al. 2005).

Here we present a preliminary modeling exercise in which a Gaussian pulse of tracer enters, with a $\sigma_t = 1$ h, the aqueous phase in the pore-space of the sediment. Three phases will be distinguished: dissolved, exchangeable in solids, and irreversibly bound to solids, corresponding to the activity concentrations C_w, $C_{s,1}$ and $C_{s,2}$. The kinetics of the uptake will be described by a first-order reversible reaction plus an irreversible and non-saturated one, with constant coefficients $k_{1,2}$, $k_{2,1}$ and $k_{2,3}$ with values 29, 46 and 0.24 h^{-1}, respectively, derived from laboratory experiments using ^{133}Ba as a tracer (Barros et al. 2005). The mathematical equivalence between parallel and consecutive reactions has been demonstrated (Barros and Abril 2008); thus, a consecutive scheme was adopted here. Because we limit ourselves to studying the time evolution of concentrations during a 1-month period,

advection and radioactive decay are not considered. Diffusion is considered only for the aqueous phase:

$$\frac{\partial C_w}{\partial t} = \frac{1}{\phi}\frac{\partial}{\partial z}\left(D_m\phi\frac{\partial}{\partial z}C_w\right) - k_{1,2}C_w + k_{2,1}C_{s,1}\frac{\rho}{\phi}$$

$$\frac{\partial C_{s,1}}{\partial t} = k_{1,2}C_w\frac{\phi}{\rho} - (k_{2,1}+k_{2,3})C_{s,1}$$

$$\frac{\partial C_{s,2}}{\partial t} = k_{2,3}C_{s,1} \tag{11}$$

For simplicity, a uniform porosity of $\phi = 0.9$ was adopted, and $\rho = \rho_s(1-\phi)$ is the bulk density, with ρ_s the density of solids (2.5 g cm^{-3}). A constant diffusion coefficient of 350 cm^2 year^{-1} was used, comparable to the value used by Robbins and Jasinski (1995).

In Fig. 5, Run-2 repeats the same exercise, but with the rate of the irreversible reaction reduced by a factor 4. In both cases, the corresponding solutions for a time simulation of 10 days and a month were identical. Thus, diffusion of tracers through the pore spaces is initially fast, but as the irreversible reaction proceeds, most of the tracer becomes irreversibly bound to solids, and the redistribution process stops. This
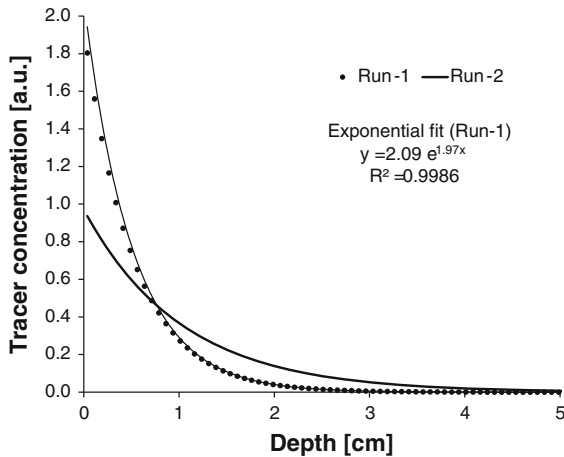

Fig. 5 Numerical solution for the kinetic-reactive-transport problem (Eq. 11), solved for a Gaussian pulse ($\sigma_t = 1$ h) of a non-radioactive tracer entering into the dissolved phase. Concentrations (in arbitrary units; a.u.) include the content of the three phases per unit dry mass of solids, and are depicted versus depth for an elapsed time of one month (Run-1, see parameter values in the text). Run-2 repeats the same exercise, but with a reduced rate of the irreversible reaction by a factor 4. The corresponding solutions for a time of simulation of 10 days and a month are identical (not shown). The dotted line corresponds to an exponential fit to Run-1

corresponds closely with the observed behavior for depth distribution patterns from the Chernobyl-derived radionuclides.

Subsurface maxima in excess ^{210}Pb profiles

Santa Barbara Basin

Koide et al. (1973) provide a description of the distribution of ^{210}Pb in a marine sediment core sampled in 1971 in the Santa Barbara Basin. The sediment had a mean water content of 84 % in the upper 10 cm and showed well defined varves that allowed development of an independent and unambiguous chronology that served to first establish the use of the ^{210}Pb radiogeo-chronology in marine sediments.

Radioactivity measurements involved counting errors of slightly >3 %. The supported fraction was estimated to be 3.5 ± 0.5 dpm g^{-1} (Koide et al. 1972). Bulk densities were estimated from the reported water and organic matter contents, assuming typical densities for inorganic solids (2.5 g cm^{-3}), organic matter (1.1 g cm^{-3}) and seawater (1.03 g cm^{-3}).

Figure 6 shows the measured ^{210}Pb$_{exc}$ versus mass depth profile, using data from Koide et al. (1973). The authors indicated that the maximum activity was near, but not at the SWI, and they suggested ^{210}Pb mobility through the interstitial waters, following changes in redox conditions, as a possible cause of this phenomenon. More recently it was shown that steep redox gradients in surface sediments may affect ^{210}Po, however, the effect of redox gradients on ^{210}Pb is limited (Kim et al. 2005).

In Fig. 6, Model-1 is the best fit to the analytical solution given by Eq. 9a, 9b, with $\phi = (831 \pm 9)$ Bq m^{-2} year^{-1}, $w = (0.067 \pm 0.001)$ g cm^{-2} year^{-1}, $g = (0.62 \pm 0.04)$ and $\alpha = (5.5 \pm 0.5)$ g^{-1} cm^2. Non-ideal deposition seems to be able to quantitatively explain the observed sub-surface maximum in ^{210}Pb$_{exc}$. Nevertheless, it can be argued that the drop in ^{210}Pb$_{exc}$ could be related to accelerated sedimentation rates, as would be expected from output of the CRS model.

Smith (2001) and others have noted that a ^{210}Pb-based chronology cannot be accepted without independent validation, and the Santa Barbara Basin core illustrates this. Ignoring the varve chronology, we can apply alternative dating models to the ^{210}Pb$_{exc}$ in Fig. 6. The common approach neglects the uppermost part of the sediment until the ^{210}Pb maximum is
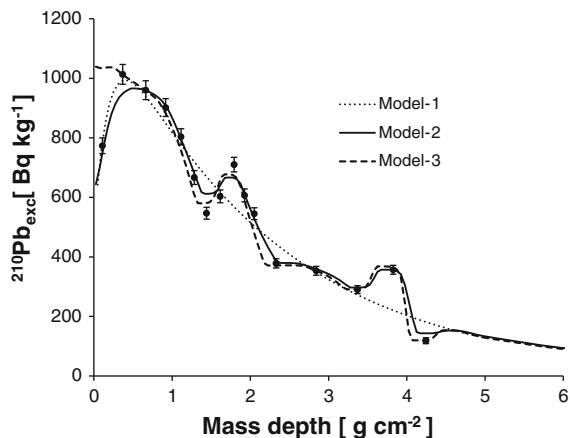
Fig. 6 $^{210}Pb_{exc}$ distribution in a sediment core from Santa Barbara Basin (34° 14.0′ N; 120° 01.5′ W; 575 m depth), sampled in 1971 (data from Koide et al. 1973, with 1 σ analytical error bars). Model-1 is the best fit to the analytical solution given by Eq. 9a, 9b with $\phi = (831 \pm 9)$ Bq m^{-2} year^{-1}, $w = (0.067 \pm 0.001)$ g cm^{-2} year^{-1}, $g = (0.62 \pm 0.04)$ and $\alpha = (5.5 \pm 0.5)$ g^{-1} cm^2. Model-2 is the numerical solution (finite differences with the MSOU scheme) of Eqs. 5–8, using $w(t)$ and fluxes from varves (Fig. 8) and $g = 0.5$, $\alpha = 5.5$ g^{-1} cm^2. Model-3 is as Model-2, but with non-ideal deposition discarded ($g = 0$)

attained and applies an exponential fit for $A(m)$. This provides $w = (0.068 \pm 0.007)$ g cm^{-2} year^{-1}, and this model explains 87 % of the observed variability in $A(m)$. Application of the CRS model, assuming incompleteness of the measured inventory (23.7 kBq m^{-2}) and correcting it by extrapolation of the exponential pattern in the deepest layers (3.6 kBq m^{-2}), leads to variable sedimentation rates, with an average value of 0.069 g cm^{-2} year^{-1} and standard deviation 0.010 g cm^{-2} year^{-1}. The best fit of Eq. 9a, 9b, which also assumes CF-CSR, leads to $w = (0.067 \pm 0.001)$ g cm^{-2} year^{-1}.

Independent validation can be sought in the chronology, and sedimentation rates, obtained from varves (Koide et al. 1973). Results are shown in Fig. 7. None of these models can be accepted, regardless of the overall statistical quality of the fits. In this particular case, as can be inferred from varves, fluxes of unsupported ^{210}Pb were not constant over time (Fig. 8). Effectively, if we assume no diffusion, as in the CRS model, then the $^{210}Pb_{exc}$ fluxes onto the sediment that correspond to the time interval defined by two consecutive varves, ϕ_i, can be obtained from the measured activity concentration in this sediment layer, A_i, the corresponding sedimentation rate, w_i, and its age T_i, from the varve chronology:
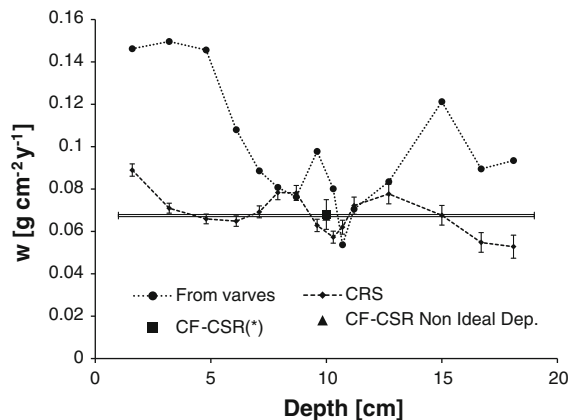

Fig. 7 Sedimentation rates versus depth for the sediment core of Santa Barbara Basin (Fig. 6) obtained from varves (Koide et al. 1973, analytical errors not provided by the authors) and three radiometric dating models: CRS, CF-CSR (omitting the first data point) and the CF-CSR with non-ideal deposition (Eq. 9a, 9b, Model-1 in Fig. 6)

$$\phi_i = A_i w_i e^{\lambda T_i} \qquad (12)$$

From Fig. 8, it is apparent that fluxes were moderately correlated with sedimentation rates, in such a way that the constant initial concentration (CIC) model could provide a basic understanding of the profile. In fact, the CIC model is closest to what Koide
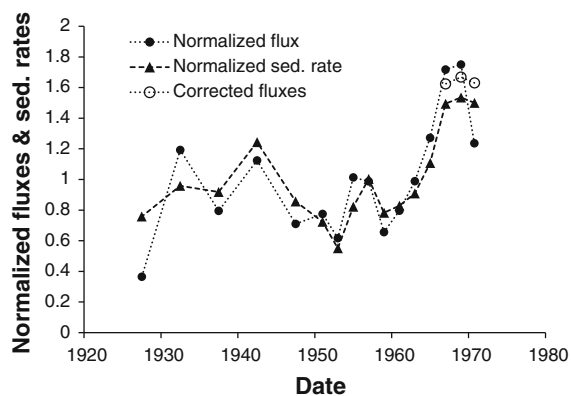

Fig. 8 Sedimentation rates from varves in the sediment core from Santa Barbara Basin (Fig. 6) versus the varve chronology (data from Koide et al. 1973). Values are normalized to their mean (0.097 g cm^{-2} year^{-1}). Estimated (by Eq. 12) excess ^{210}Pb fluxes are also depicted (normalized to their mean value of 936 Bq m^{-2} year^{-1}). Circles correspond to the estimated corrected values for fluxes (by extrapolation of the ϕ/w ratio from immediate adjacent layers) to remove the effect of non-ideal deposition in the uppermost sediment layers

et al. (1973) did in their paper, plotting total ^{210}Pb activity versus varve chronology. Nevertheless, if the varve chronology is ignored, the selection of the value of the initial concentration in the CIC model will be critical in this example, as a consequence of the subsurface maximum.

The goal now is to show how the subsurface maximum can be understood from Eqs. 5–7 and assumptions of Eq. 8. The time series of sedimentation rates and fluxes derived from the varve chronology will be taken into account (Fig. 8), to avoid erroneous assumptions about these magnitudes. The only required refinement is to discard the fluxes estimated by Eq. 12 in the uppermost sediment layers, because they will be noticeably affected by non-ideal deposition. Corrected values for fluxes were estimated in Fig. 8 by extrapolation of the ϕ/w ratio from immediate adjacent layers. For the remaining sediment core, $\alpha \gg \lambda/w$ so that Eq. 12 provides a good estimate of fluxes.

In Fig. 6, Model-2 is the numerical solution, finite differences with MSOU scheme, using Eqs. 5–8 and estimates of $w(t)$ and fluxes from the varve data (Fig. 8) and $g = 0.5$, $\alpha = 5.5$ g^{-1} cm^2. The model reasonably reproduces the measured ^{210}Pb$_{exc}$ profile, particularly the subsurface maximum. For the sake of comparison, Model-3 is provided as the corresponding numerical solution when non-ideal deposition is discarded ($g = 0$). In this case the subsurface maximum cannot be reproduced.

The parameter set describing the subsurface maximum indicates that some 50 % of the excess ^{210}Pb input is delivered as non-ideal deposition, which can be described as an exponential penetration pattern with a scaling factor of 1.2 cm^{-1}. Even under conditions of time-dependent sedimentation rates and fluxes, the use of constant values can provide, when co-variation such as described in Fig. 8 is applicable, a reasonable tool to describe non-ideal deposition patterns.

Core from Baja California

The second example also comes from Koide et al. (1973) and corresponds to a sediment core from Baja California (No. 224, 25°13.8′N; 112°40.6′W; 520 m depth). Water content was >80 % in the topmost 6 cm. Non-varved structures were observed in this core. Associated errors in the ^{210}Pb measurements were ∼3 %. The length of the core allowed estimation of supported ^{210}Pb from values in the deepest layers, and the bulk densities were obtained as in the previous case. This core also showed a well-defined sub-surface peak in ^{210}Pb$_{exc}$. Figure 9a shows the best fit obtained using the analytical solution given by Eq. 9a, 9b and
$\phi = (610 \pm 6)$ Bq m^{-2} year^{-1},
$w = (0.054 \pm 0.01)$ g cm^{-2} year^{-1},
$g = 0.68 \pm 0.03$ and $\alpha = (4.4 \pm 0.2)$ g^{-1} cm^2. As the authors noted, the constant ^{210}Pb value between 1.9 and 3.9 g cm^{-2} mass depth might reflect a slump. In this example, the values of the parameters describing the non-ideal deposition pattern are comparable to those of the Santa Barbara Basin.

Skan Bay sediments

Sugai et al. (1994) reported depth distributions of ^{210}Pb and ^{137}Cs in sediment cores from Skan Bay, Alaska, collected between 1980 and 1990. The sediment porosity was very high (>0.97) near the SWI, and remained ∼0.88 above a mass depth of 2 g cm^{-2}. X-radiographs revealed distinct layers, and hence continuous mixing by bioturbation was ruled out. However, ^{210}Pb$_{exc}$ profiles from 1984, 1987 and 1990 showed an activity maximum slightly below the SWI. Comparison of ^{137}Cs profiles during this period of time, through numerical modelling, was consistent with the hypothesis of little or no diffusion. The authors concluded that the cause of maximum ^{210}Pb concentrations slightly below the SWI was unknown.

Figure 9b shows the ^{210}Pb$_{exc}$ profile for the core sampled in 1987, which was free of any episodic deposition event that could have affected the other cores, as the authors claimed. The analytical solution given by Eq. 9a, 9b provides a good fit to this data ($\chi = 0.81$). In this example, the fraction of the flux undergoing non-ideal deposition was estimated to be lower (27 %), and the penetration depth larger, with a scaling factor of 2.4 cm^{-1}.

The measured ^{137}Cs profile will not be treated here, because its quantitative modelling requires handling the appropriate time-dependent input functions, which probably are governed in this case by the Integrated Atmospheric Flux effect (Abril and García-León 1994) or by the System-Time-Averaged effect (Robbins et al. 2000).
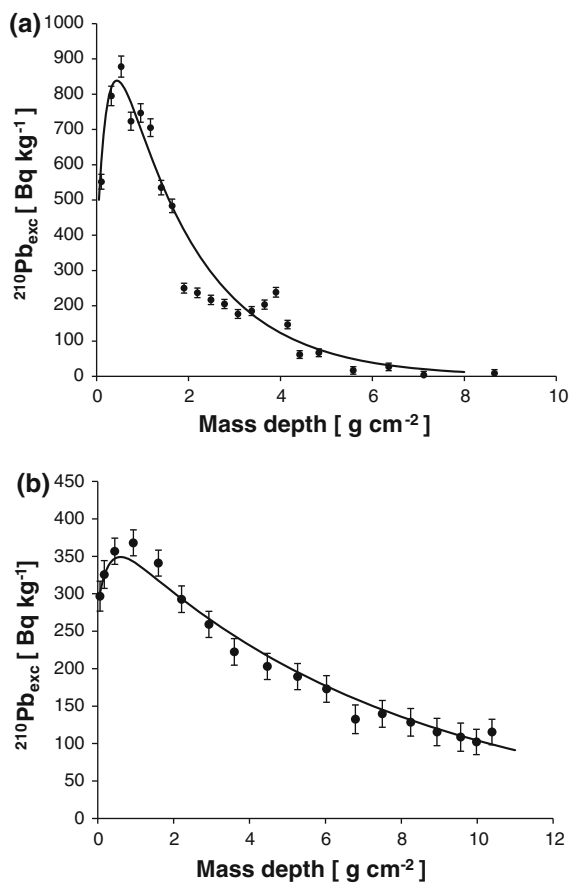
Fig. 9 Measured $^{210}Pb_{exc}$ versus mass depth profile and analytical fits (to Eq. 9a, 9b) for: **a** a sediment core from Baja California (224, 25° 13.8′N; 112° 40.6′W; 520 m depth; data from Koide et al. 1973) with $\phi = (610 \pm 6)$ Bq m^{-2} year^{-1}, $w = (0.054 \pm 0.01)$ g cm^{-2} year^{-1}, $g = 0.68 \pm 0.03$ and $\alpha = (4.4 \pm 0.2)$ g^{-1} cm^2; **b** core 87A sampled in 1987 in Skan Bay (Sugai et al. 1994), with $\phi = (915 \pm 16)$ Bq m^{-2} year^{-1}, $w = (0.235 \pm 0.006)$ g cm^{-2} year^{-1}, $g = 0.27 \pm 0.05$ and $\alpha = (3.4 \pm 1.0)$ g^{-1} cm^2 ($\chi = 0.81$)

Discussion

The selected examples of deposition patterns for Chernobyl-derived radionuclides show large and rapid penetration into the surface sediment, which cannot be consistently described by one or two-phase equilibrium models, particularly when a sequence of sampling dates is considered. For the Baltic Sea sediments (Fig. 4) it could be argued that site-to-site variability might justify use of different diffusion coefficients (following Eq. 10, but with appropriate parameter values) to explain both profiles. Nevertheless, the need for decreasing diffusion coefficients with time seems

to have a general application, as in the case of Robbins and Jasinski (1995). The same effect has been invoked for interpretation of depth distributions of Chernobyl radionuclides in soils, in terms of apparent advection and diffusion (Almgren and Isaksson 2006). Likewise, it is invoked for laboratory experiments carried out with replicated sediment columns with different contact times under a "traced water body" (Barros et al. 2005). It seems likely that the initial diffusion coefficients were overestimated as a mathematical artifact to compensate for other fast redistribution processes that fall beyond the model capabilities. Profiles in Figs. 3–4 are more reasonably explained by a one-phase model that incorporates non-ideal deposition.

Kinetic reactive transport seems to be a good candidate to explain the physical–chemical processes behind non-ideal deposition. An exponential penetration pattern seems to be a reasonable approach to describe non-ideal deposition when diffusion is limited to the aqueous phase in the pore space, as shown in Fig. 5.

When settled particles already carry an irreversibly bound fraction of the tracer, which is also present in dissolved form, a fractioning of the global input (factor g in Eqs. 6–7) naturally arises, although other causes for partitioning may be possible. In fact, the idea of a partitioning of the radioactive flux into the sediment has been used for dating purposes with the Incomplete Mixing Zone (IMZ) model (Abril et al. 1992; Abril 2003b, 2004; Erlinger et al. 2008).

Other processes may also explain non-ideal deposition patterns. Abril (2011) demonstrated that the ubiquitous steep gradients in bulk density profiles in surface sediments can be understood in terms of a transport equation governed by gravity and depth-dependent conductivity. Early compaction is a phenomenon of reallocation of solid particles towards a higher packing order, under the action of stirring and the gravitational field. The associated mass flow decreases with depth until it vanishes at the early-compaction limit. In this scenario, a limited conduction of colloidal and small-size particles is not surprising. Migration of colloidal particles through macropores is a well known phenomenon in soil physics and it has been shown that the transport of radionuclides can be unexpectedly fast in dry soils with high clay content as a consequence of mass flows in cracks (Al-Masri 2006; Almgren and Isaksson

2006). Nevertheless, experimental evidence for a similar phenomenon affecting saturated sediments has not yet been described.

At the miscroscale, the SWI is not an ideal layer, but it adapts to the rugose surface and penetrates into the sediment through the larger pore spaces. The role of this "expanded" surface in the direct uptake of tracers from the overlying water column has been described by Barros et al. (2005). The extent to which this and other physical and chemical factors such as changes in redox conditions, can contribute to non-ideal deposition patters is not yet well understood. From the physical–chemical nature of these processes, it is expected that non-ideal deposition can also affect $^{210}Pb_{exc}$ profiles. Here the penetrating tails cannot be directly recognized, but as shown above, they may be responsible for the often-observed sub-surface maxima.

Sub-surface maxima in $^{210}Pb_{exc}$ profiles can be the combined effect of depth-penetration of fluxes and accretion. It can be shown that the particular formulation of $s(m)$ is not critical; thus, subsurface maxima also appear when using a Fermi-type distribution, as in Eq. 10. From the current understanding of these penetration patterns, it can be expected that they will be present to some extent in most cases, but cannot always be easily recognized. Non-ideal deposition patterns in $^{210}Pb_{exc}$ profiles can be hidden because of low resolution in sectioning of the core, or because of large counting errors. The fraction of the flux undergoing non-ideal deposition and/or the penetration depth can be small, or their combination can result in exponential decay or acceleration patters (Fig. 1).

The situation is even more complex with man-made radionuclides, because of time-dependent atmospheric deposition, and pre-depositional processes that govern the fluxes that finally enter the sediment. The maximum penetration depth has often been used as a time marker in ^{137}Cs chronologies, i.e. the beginning of the 1950s. In cases where non-ideal deposition is relevant, this approach could lead to wrong results.

Conclusions

Typical boundary conditions, explicitly or implicitly assumed in the one-phase radiometric dating models for recent sediments, impose the continuity of fluxes at the SWI under the assumption of ideal deposition. That is, radiotracers are particle-bound and any new input is necessarily deposited atop previously existing material, after which diffusive processes, if they exist, may proceed. This mathematical condition does not reflect appropriately the physical processes in sediments with high porosity and/or with inputs of radiotracers with a large dissolved fraction. High ^{137}Cs inputs following the Chernobyl accident generated depth distribution patterns in some sediment cores that cannot be explained by bioturbation and diffusion used in one- and two-phase equilibrium models.

A deposition process in which a fraction of the radioactive input is distributed with depth, rapidly when compared with sedimentation rates, seems to be more realistic. This fast penetration could be partially explained by, among other factors, kinetic reactive transport processes within the sediment. Mathematically, this can be described as a depth-dependent source term in the governing mass-conservation equation used in one-phase radiometric dating models.

Non-ideal deposition patterns can explain the existence of sub-surface maxima in $^{210}Pb_{exc}$ profiles, and the penetrating tails in ^{137}Cs profiles, as shown with some examples from the literature in which sediment porosities were >90 %. In many situations, non-ideal deposition patterns, even when they exist, can hardly be recognized if they are of low or very high intensity, or when they act in combination with other pre- and post-depositional redistribution processes. Some problems in radiometric dating caused by non-ideal deposition are the spurious acceleration of sedimentation inferred when applying the CRS model and erroneous chronologies developed using the maximum penetration depth of ^{137}Cs in profiles as a time marker.

References

Abril JM (2003a) A new theoretical treatment of compaction and the advective-diffusive processes in sediments. A reviewed basis for radiometric dating models. J Paleolimnol 30:363–370

Abril JM (2003b) Difficulties in interpreting fast mixing in the radiometric dating of sediments using ^{210}Pb and ^{137}Cs. J Paleolimnol 30:407–414

Abril JM (2004) Constraints on the use of Cs-137 as a time-marker to support CRS and SIT chronologies. Environ Pollut 129:31–37

Abril JM (2011) Could bulk density profiles provide information on recent sedimentation rates? J Paleolimnol 46:173–186

Abril JM, García-León M (1994) The integrated atmospheric flux effect in a radiogeochronological model. J Environ Radioact 24:65–79

Abril JM, García-León M, García-Tenorio R, Sánchez CI, El-Daoushy F (1992) Dating of marine sediments by an incomplete mixing model. J Environ Radioact 15:135–151

Al-Masri MS (2006) Vertical distribution and inventories of ^{137}Cs in the Syrian soils of the eastern Mediterranean region. J Environ Radioact 86:187–198

Almgren S, Isaksson M (2006) Vertical migration studies of ^{137}Cs from nuclear weapons fallout and the Chernobyl accident. J Environ Radioact 91:90–102

Appleby PG, Oldfield F (1978) The concentration of lead-210 dates assuming a constant rate of supply of unsupported ^{210}Pb to the sediment. Catena 5:1–8

Barros H, Abril JM (2008) Kinetic box models for the uptake of radionuclides and heavy metals by suspended particulate matter: equivalence between models and its implications. J Environ Radioact 99:146–158

Barros H, Abril JM, El-Mrabet R, Laissaoui A (2005) Kinetically controlled radionuclide sorption by sediment cores from two different environments. In: Méndez-Vilas A (ed) Experimental studies using 133Ba as a tracer. Applied physics (APHYS 2003). Elsevier, Amsterdam, pp 531–542

Baskaran M, Naidu AS (1995) ^{210}Pb-derived chronology and the fluxes of ^{210}Pb and ^{137}Cs isotopes into continental shelf sediments, East Chukchi Sea, Alaskan Artic. Geochim Cosmochim Acta 59:4435–4448

Belluci LG, Frignani M, Cochran JK, Albertazzi S, Zaggia L, Cecconi G, Hopkins H (2007) ^{210}Pb and ^{137}Cs chronometers for salt marsh accretion in the Venice-Lagoon—links to flooding frequency and climate change. J Environ Radioact 97:85–102

Christensen ER (1982) A model for radionuclides in sediments influenced by mixing and compaction. J Geophys Res 87:566–572

El-Mrabet R, Abril JM, Manjón G, García-Tenorio R (2001) Experimental and modelling study of the Plutonium uptake by suspended matter in aquatic environments from the south of Spain. Water Res 35:4184–4190

Erlinger Ch, Lettner H, Hubmer A, Hofmann W, Steinhäusler F (2008) Determining the Chernobyl impact on sediments of a pre-Alpine lake with a very comprehensive set of data. J Environ Radioact 99:1294–1301

Evans DW, Alberts JJ, Clark RA (1983) Reversible ion-exchange fixation of caesium-137 leading to mobilization from reservoir sediments. Geochim Cosmochim Acta 47:1041–1049

Fukumori E, Christensen ER, Klein RJ (1992) A model of ^{137}Cs and other tracers in lake sediments considering particle size and the inverse solution. Earth Planet Sci Lett 114:85–99

Fuller CC, van Geen A, Baskaran M, Anima R (1999) Sediment chronology in San Francisco Bay, California, defined by ^{210}Pb, ^{234}Th, ^{137}Cs and ^{239,240}Pu. Mar Chem 64:7–27

Holby O, Evans S (1996) The vertical distribution of Chernobyl-derived radionuclides in a Baltic Sea sediment. J Environ Radioact 33:129–145

Kim G, Kim SJ, Harada K, Schultz MK, Burnett WC (2005) Enrichment of excess ^{210}Po in anoxic ponds. Environ Sci Technol 29:4894–4899

Koide M, Soutar A, Goldberg ED (1972) Marine geochronology with ^{210}Pb. Earth Planet Sci Lett 14:442–446

Koide M, Bruland K, Goldberg ED (1973) Th-228/Th-232 and Pb-210 geochronologies in marine and lake sediments. Geochim Cosmochim Acta 37:1171–1187

Kramer KJM, Misdorp R, Berger G, Duijts R (1991) Maximum pollutant concentrations at the wrong depth: a misleading pollution history in a sediment core. Mar Chem 36:183–198

Laissaoui A, Benmansour M, Ziad N, Ibn Majah M, Abril JM, Mulsow S (2008) Anthropogenic radionuclides in the water column and a sediment core from the Alboran Sea: application to radiometric dating and reconstruction of historical water column radionuclide concentrations. J Paleolimnol 40:823–833

Meysman FJR, Boudreau BP, Middelburg JJ (2005) Modeling reactive transport in sediments subject to bioturbation and compaction. Geochim Cosmochim Acta 69:3601–3617

Periáñez R (2005) Modelling the dispersion of radionuclides in the marine environment. An introduction. Springer, Berlin

Petersen W, Knauth HD, Pepelnik R (1990) Vertical distribution of Chernobyl isotopes and their correlation with heavy metals and organic carbon in sediment cores of the Elbe Estuary. Sci Total Environ 97:531–547

Robbins JA (1978) Geochemical and geophysical applications of radioactive lead isotopes. In: Nriago JO (ed) Biochemistry of lead in the environment. Elsevier, Amsterdam, pp 285–393

Robbins JA, Jasinski AW (1995) Chernobyl fallout radionuclides in Lake Sniardwy, Poland. J Environ Radioact 26:157–184

Robbins JA, Holmes C, Halley R, Bothner M, Shinn E, Graney J, Keeler G, tenBrink M, Orlandini KA, Rudnick D (2000) Time-averaged fluxes of lead and fallout radionuclides to sediments in Florida Bay. J Geophys Res 105:28805–28821

Smith JN (2001) Why should we believe ^{210}Pb sediment geochronologies? J Environ Radioact 55:121–123

Sugai SF, Alperin MJ, Reeburgh WS (1994) Episodic deposition and ^{137}Cs immobility in Skan Bay sediments: a ten-year ^{210}Pb and ^{137}Cs time series. Mar Geol 116:351–372